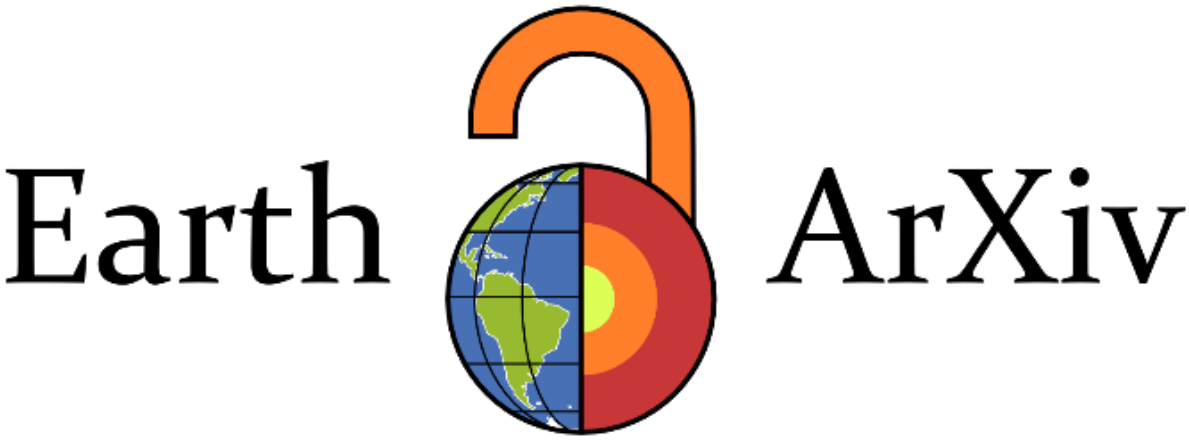

Assessing the Predictive Skill of Global Climate Models for Long and Short Rains in the Greater Horn of Africa

Athanase Hafashimana[1*], Mouhamadou Bamba Sylla[2†], Philibert Nsengiyumva[3†], Masilin Gudoshava[4†], Martin Kuradusenge[5], Richard Kabanda[6]

[1*]Data Science, African Centre of Excellence in Data Science, University of Rwanda, KK 737, Kigali, P.O. Box: 4285, Rwanda.
[2]Climate Change Science, AIMS Research and Innovation Centre, Rue KG590 ST 1, Kigali, P.O. Box: 6428, Rwanda.
[3]Electrical Engineering, College of Science and Technology, University of Rwanda, KN 7, Kigali, P.O. Box: 3900, Rwanda.
[4]Climate Science, IGAD Climate Prediction and Applications Centre, Nairobi, P.O. Box: 10304-00100, Kenya.
[5]Information Systems, College of Science and Technology, University of Rwanda, KN 7, Kigali, P.O. Box: 3900, Rwanda.
[6]Economics, College of Business and Economics, KK 737, Kigali, P.O. Box: 4285, Rwanda.

*Corresponding author(s). E-mail(s): ahafashimana@aimsric.org;
Contributing authors: msylla@aimsric.org; p.nsengiyumva@ur.ac.rw; Masilin.Gudoshava@igad.int; m.kuradusenge@ur.ac.rw; r.kabanda@ur.ac.rw;
†These authors contributed equally to this work.

Abstract

Seasonal forecasts play a crucial role in delivering early warnings to various sectors, particularly the agricultural sector. The Greater Horn of Africa region depends on rainfed agriculture, hence the need for accurate forecasts. This study uses Global Climate Models (GCMs) and satellite precipitation observations to assess the predictability of observed precipitation by deploying traditional

machine learning algorithms and deep learning models. We compare the predictability of long and short rainy seasons in the region. The results highlight the challenges of forecasting the long rains season, with traditional machine learning algorithms showing low feature importance. In contrast, short rains can be predicted and achieved with high accuracy using both traditional machine learning models and deep learning architectures, particularly Long Short-Term Memory (LSTM) networks. In this study, we used ten Global Climate Models as input features for seasonal climatological forecasts, with a single output feature derived from observations of the Global Precipitation Climatology Center (GPCC) over a 30-year period (1990-2019). We measured the level of explained variance of this set of GCMs. Regardless of the method, high explainable variability was achieved in short rains, and the European Centre for Medium-Range Weather Forecasts (ECMWF) was the best predictor in the region for long rains. On the other hand, the National Aeronautics and Space Administration (NASA) was the most significant contributor to the predictions for short rains.

1 Introduction

Seasonal forecasting (SF) serves as valuable information for a number of climate sensitive sectors including agriculture, disaster risk management, water and health among others(Klemm & McPherson, 2017). These forecasts have been used for strategic planning by the different stakeholders. In addition, SF is used in policy and decision-making processes to inform stakeholders about predicted climate variability and change (Bruno Soares, Daly, & Dessai, 2018). It is evident that the productivity and profitability of agriculture depend on weather and SF information (Paparrizos, Attoh, Sutanto, Snoeren, & Ludwig, 2023). Although SF plays an important role in agriculture, the interdependence of rainfall and surface temperature influences most practices, from the sowing stage to the harvest stage (J. Liu, Fu, & Liu, 2023; Talib, Ahmed, Naseer, Slusarczyk, & Popp, 2021; Zhang, Sun, Singh, & Chen, 2012). In different parts of the world, agricultural machinery such as irrigation is being used to increase agricultural productivity (Ringler, Mekonnen, Xie, & Uhunamure, 2020). This practice may be a game changer for rainfed agricultural regions, but poses a financial constraint for many African countries (Harmon, Jepson, & Lefore, 2023; Nhamo et al., 2024; Pfunzo, Bahta, & Jordaan, 2024). Therefore, SF is needed to inform both rainfed farmers and mechanized agricultural investors (Hounnou, Houessou, & Dedehouanou, 2023; Ingram, Roncoli, & Kirshen, 2002).

Although an SF is issued for different fields, including strategic planning of agricultural practices, timely data availability is a tangible asset for scientists in agrometeorological services (Bacci et al., 2023; Bacci, Ousman Baoua, & Tarchiani, 2020; Vuković Vimić et al., 2022). This availability is attributed to Global Climate Models (GCMs), which are physical representations of the interaction between land, ocean, and atmosphere to simulate a specific climate variable at each point on the grid in the world (Assamnew & Tsidu, 2020; Joshi, Gouda, & Goswami, 2020). In addition, reliable data sources are essential to generate accurate seasonal forecasts. Some of them

include the Copernicus Climate Change Service (C3S), which stores the output from the European Center for Medium-Range Weather Forecasts (ECMWF), Météorologie Nationale Française (Météo-France), Deutscher Wetterdienst (DWD), Centro Euro-Mediterraneo sui Cambiamenti Climatici (CMCC) (Calì Quaglia, Terzago, & von Hardenberg, 2022; Gebrechorkos, Pan, Beck, & Sheffield, 2022; Kim et al., 2021). Moreover, GCM data sets from the Columbia University International Research Institute for Climate and Society (IRI) Data Library serve to provide various outputs such as the NASA Global Earth Observing System Seasonal to Subseasonal Prediction System (NASA-GEOSS2S), Geophysical Fluid Dynamics Laboratory Seamless System for Prediction and Earth System Research (GFDL-SPEAR), Community Climate System Model Version 4 (CCSM4) (Ehsan et al., 2021; Giannini et al., 2020; Pakdaman, Babaeian, & Bouwer, 2022). Furthermore, the World Meteorological Organization (WMO) has various GCMs. Some of them include the China Meteorological Administration (CMA), the Centro de Previso de Tempoe Estudos Climáticos (CPTEC), the Korea Meteorological Administration (KMA), the Japan Meteorological Agency (JMA), in addition to those stated for the C3S and IRI data library (Reboita, Mattos, Capucin, de Souza, & de Souza Ferreira, 2024; Shu et al., 2021; Taguchi, 2018).

We make use of the availability of data and the development of predictive algorithms. When predicting a single output feature for a given single input feature, simple linear regression is useful. Considering multiple features, other linear models with regularization properties, such as ridge and Lasso regression. As we move forward, we could even train traditional machine learning algorithms that have nonlinear objective functions. These methods include Random Forest, Decision Trees, Extreme Gradient Boosting, and Support Vector Regression with nonlinear kernels (Anwar, Winarno, Hadikurniawati, & Novita, 2021; Kumar, Kedam, Sharma, Khedher, & Alluqmani, 2023; Li et al., 2023; Sattari, Feizi, Samadianfard, Falsafian, & Salwana, 2021). Despite the ability of traditional machine learning algorithms to predict climate variables, an algorithm such as support vector regression struggles with nonlinear precipitation patterns (M. Wang et al., 2024). Moreover, traditional machine learning models often require meticulous feature engineering, yet only a few methods such as gradient boosting demonstrate relatively consistent success in capturing complex climate patterns (He, Li, DelSole, Ravikumar, & Banerjee, 2020). Furthermore, these methods face the challenge of handling the high-dimensional predictor matrix in the case of many features (Lin, Fan, Hou, & Wang, 2023). These limitations have led to the adoption of deep learning architectures, such as the Multi-Layer Perceptron (MLP). Since climate data are sequence-based records, neural networks such as Long Short-Term Memory (LSTM) are useful. This technique relies on training weights with backpropagation to achieve better results. In predicting precipitation, a few layers are needed to achieve robust seasonal forecasts. Using stacking architectures beyond two layers diminishes the predictive skill of LSTM models in forecasting seasonal precipitation (Akbar, Darmawan, Wibowo, & Rahmat, 2024; Barrera-Animas et al., 2022).

The use of machine learning and deep learning models in weather and seasonal precipitation forecasts in different parts of the world is becoming a critical idea to define robustness in this field (Basha, Bhavana, Bhavya, & Sowmya, 2020; Jin et al., 2022).

In the prediction process, dynamical models provide different outputs under different initial conditions. The beam formulated on averaging these candidate outputs can better predict signals that stand out from the noise of individual weather events. This led to the evolution of hybrid-based seasonal forecasting that combines the dynamical ensemble output with statistical or machine learning approaches (Fuentes-Franco, Giorgi, Pavia, Graef, & Coppola, 2018; Gibson et al., 2021). These hybrid-based seasonal forecasts are fueled by the existence of multi-model ensembles from different originating centers. Some of them are the Copernicus Climate Change Service (C3S), and the North American Multimodel Ensemble (NMME) (Becker, Kirtman, & Pegion, 2020; Manzanas et al., 2019). Although machine learning approaches are widely used, climate forecasters were aware of the minimum prediction bias when comparing the average of the ensemble members with the target observation. According to (Kassem, Gökçekuş, Çamur, & Esenel, 2021), the coefficient of determination (R^2) outperforms bias-based metrics such as the root mean square error (RMSE) and the mean absolute error (MAE) when evaluating the performance of traditional machine learning and deep learning models.

Despite the fact that the average of the ensemble members can produce better prediction metrics when dealing with hybrid-based seasonal precipitation forecasting, seasonal variability may be a source of low explained variance (Izadi et al., 2021). Considering a specific region such as the Greater Horn of Africa (GHA), there are different seasons for which we can have short rains that extend from October to December (OND) and long rains that extend from March to May (MAM) (Schwarzwald, Goddard, Seager, Ting, & Marvel, 2023). These definitions were introduced in the early 2000s based on climatological studies in East African countries. The term "long rains" originated in Kenya to describe rainfall during the MAM season, which typically features extended periods of more intense precipitation than the short rains of OND (Camberlin & Philippon, 2002), while the term "short rains" originated in Uganda to describe rainfall during OND season, which features shorter duration and less intense received rainfall compared to the MAM season (Mubialiwo, Onyutha, & Abebe, 2020). According to (Anyah & Qiu, 2012), the seasonal variability over the Greater Horn of Africa (GHA) and the climatological characteristics of precipitation indicate that the Coupled Model Intercomparison Project (CMIP) tends to overestimate the peak of the October–November–December (OND) season. However, for the March–April–May (MAM) season, the models incorrectly identify May as the peak month, which does not align with the observations. This shift in the maximum value during the long rains of the region could introduce challenges in precipitation prediction, as the signal may not align at specific grid points. Consequently, the March–April–May (MAM) season has been characterized by low forecast skill, limiting its usefulness for climate services and decision-making (Antonio et al., 2025; Daron et al., 2025; Deman et al., 2022; Ward et al., 2023). The Greater Horn of Africa (GHA) region may also experience significant seasonal variability influenced by large-scale climate teleconnections, particularly El Niño and La Niña events (Mpelasoka, Awange, & Zerihun, 2018). The October–December (OND) season is characterized by greater interannual variability compared to the March–April–May (MAM) season in the Greater Horn of Africa region. This variability is strongly influenced by large-scale climate phenomena such

as the El Niño–Southern Oscillation (ENSO) and the Indian Ocean Dipole (IOD) (Bowden & Semazzi, 2007; MacLeod, Graham, O'Reilly, Otieno, & Todd, 2021).

The influence of ENSO on rainfall over the Greater Horn of Africa is more pronounced during the short rains than the long rains (Palmer et al., 2023). Positive phases of the IOD, particularly when coinciding with El Niño events, are associated with substantial increases in precipitation, often resulting in extreme rainfall anomalies (Funk et al., 2018; Jiang, Zhou, Roundy, Hua, & Raghavendra, 2021; Nicholson, 2015). Conversely, the long rains exhibit a weaker and less consistent response to these climate drivers, suggesting a more complex interplay of regional and global factors. These findings indicate that the short rains are more sensitive to IOD and ENSO variability, offering greater potential for seasonal predictability (Kebacho, 2022a; Vellinga & Milton, 2018). In addition, there are local drivers of the variability of long and short rains in the Greater Horn of Africa. According to (Dyer & Washington, 2021; Kebacho, 2022b; Kilavi et al., 2018; Martin et al., 2021; Vellinga & Milton, 2018), Western Indian Ocean Sea Surface Temperature (SST) anomalies enhance both long and short rains by promoting atmospheric ascent. Positive SSTs drive over 95% of short rain increases and 9–26% of long rain variability. Tropical cyclones and Congo Basin westerlies, often linked to Madden–Julian Oscillation (MJO) phases 3–4, further influence rainfall patterns. Stronger zonal and surface westerlies correlate with wetter long rains, especially over Tanzania and Lake Victoria.

Given that the World Meteorological Organization (WMO) recommended objective forecasting systems, we will use machine learning and deep learning approaches to determine which models are best suited for each season. The main objective of this study is to evaluate the performance of individual GCMs as features of prediction of the observed climatology for the MAM and OND seasons. Moreover, to determine the explained variance of the set of GCMs while predicting seasonal rainfall in the Greater Horn of Africa for the MAM and OND seasons. Furthermore, we quantify the contribution of each ensemble mean from the reporting centre to seasonal precipitation predictions, highlighting the representativeness and relative importance of individual GCMs across the seasons. In fact, we want to determine a suitable machine learning algorithm or deep learning architecture on regression tasks for a specific season over the set of predictive models considered.

2 Data and Study Area

2.1 Data

The data in Table 1 provide details about the ensemble members of a specific global climate model (GCM). The number of members in the forecast and hindcast ensemble are represented by **F_ENS** and **H_ENS** respectively. The lead time, horizontal resolution, and temporal resolution are represented by **L_T**, **H_Res**, and **T_Res** respectively. The GCMs originate from different sources. These include the International Research Institute for Climate and Society data library at Columbia University abbreviated as (IRI DL) and the Copernicus Climate Change Service (C3S). In the representation of GCM, all members contributed in the ensemble average. The GCMs were regridded with the observed data, Global Precipitation Climatology Center (GPCC), with

a resolution of $0.5° \times 0.5°$. According to (Devadarshini et al., 2024; Hartmann, 2025), regridding is always necessary for the actual matching of the grid points of two or more GCMs to be compared to the observed target precipitation reporting centre.

Table 1: Summary of the data used

Source	GCM	F_Ens	H_Ens	L_T	H_Res	T_Res
C3S	ECMWF	51	25	3	$1° \times 1°$	Monthly
IRI DL	NASA	10	4	3	$1° \times 1°$	Monthly
C3S	Météo France	51	25	3	$1° \times 1°$	Monthly
IRI DL	GFDL_SPEAR	30	15	3	$1° \times 1°$	Monthly
C3S	DWD	50	30	3	$1° \times 1°$	Monthly
IRI DL	ColaCCSM4	10	10	3	$1° \times 1°$	Monthly
C3S	CMCC	50	40	3	$1° \times 1°$	Monthly
IRI DL	CanSIPS-IC4	40	40	3	$1° \times 1°$	Monthly
C3S	NCEP	28	24	3	$1° \times 1°$	Monthly
C3S	ECCC	21	10	3	$1° \times 1°$	Monthly
Source	**Observation**	-	-	-	-	-
C3S	GPCC	-	-	-	$0.5° \times 0.5°$	Monthly

2.2 Study Area

Greater Horn of Africa is the region located in the eastern and some central parts of Africa. It is situated between $20°E - 52°E$ longitudes and $13.5°S - 25°N$ latitudes. It comprises 11 countries, such as Burundi, Djibouti, Eritrea, Ethiopia, Kenya, Rwanda, Somalia, Tanzania, South Sudan, Sudan, and Uganda. Most countries in the region are tropical and may experience heavy rains during their respective long rains. In addition, a country like Sudan that is part of the Sahel region can face the effect of the Sahara desert, such as limited moisture and humidity that leads to a very small amount of rainfall received compared to other countries that are not directly exposed (Mohamed, Maharana, Phartyal, & Dimri, 2024).

Taking into account the entire year, the percentage contribution of the MAM season appears to be the main contributor, followed by the OND, to the total annual rainfall received in the region (Misiani et al., 2025). The spatial signal may differ in amount and intensity due to various factors, such as topography. Some places may receive orographic rainfall; that cannot be the case in the lowlands (Basist, Bell, & Meentemeyer, 1994; Oettli & Camberlin, 2005; Shetty, Umesh, & Shetty, 2022). Moreover, the availability of large water bodies may cause the difference. If the region is directly exposed to the lake or ocean, it is expected to have a different rainfall pattern from arid areas such as the various parts of Sudan (Agbasi et al., 2023; Ibebuchi & Abu, 2023). Furthermore, vegetation cover in a specific region can influence the amount of rainfall received and is generally involved in the entire water cycle, mainly transpiration as part of the process (Jingyong, Wenjie, Congbin, & Lingyun, 2003). The veracity of both the water bodies and the vegetation cover can lead to an analysis

of received rainfall and evapotranspiration in the water cycle of the region (Kirchner & Allen, 2020). In the following **Figure 1**, we have a spatial representation of the countries that we designed using geographical boundaries in the shapefile of the region.

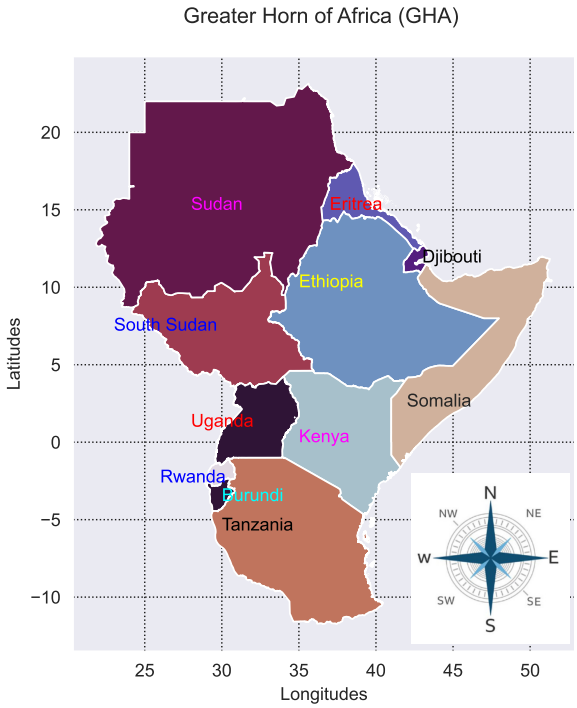

Fig. 1: Member countries of GHA

3 Study Setup and Methods

3.1 Conceptual Framework and Specification of the Setup

In this section, we explain the general setup of our experiment based on the standard functional relationship between GCMs and satellite observations for the OND and MAM seasons. In fact, the theoretical framework for this study is based on the evaluation of the effect of GCM on the observed seasonal average of the total precipitation rate through the relationship between GCMs, as independent variables, and the observed precipitation values of GPCC, as a dependent variable. Each predictive model is trained on 10 different input features. All features originate from the same forecasting centres throughout the two seasons detailed in Table 1. Spatial distribution of grid values for the input and output features is presented in the Figures 2 and 3.

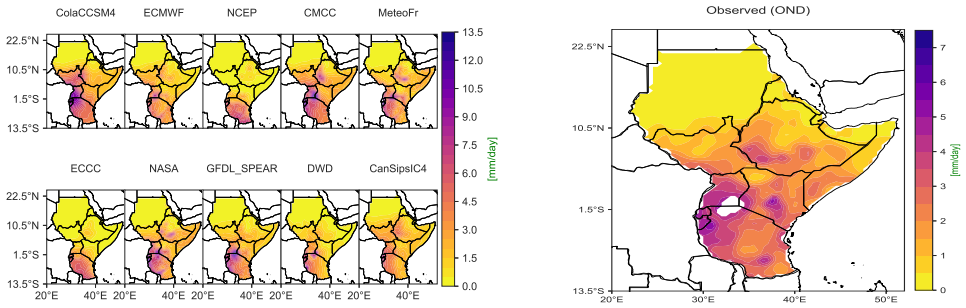

(a) (b)

Fig. 2: Grid values of GCMs considered as features of the OND season in (a) and observed values from GPCC in (b).

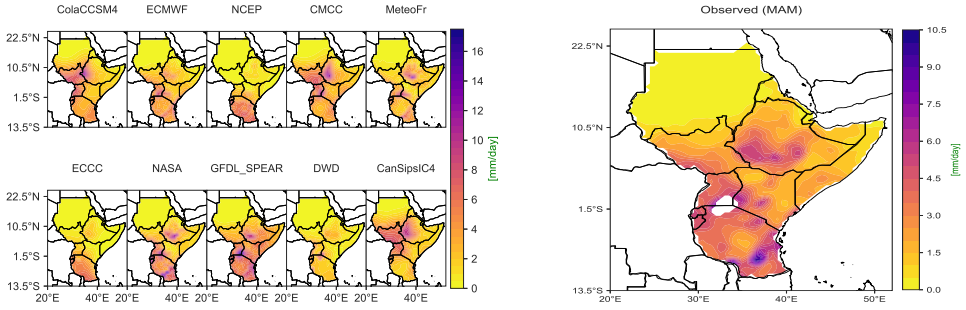

(a) (b)

Fig. 3: Grid values of GCMs considered as features of the MAM season in (a) and observed values from GPCC in (b).

Figures 2 and 3 show the seasonal precipitation forecasts from GCMs as predictors of the observed short and long rains respectively. These features are the spatial distribution of the precipitation rate values from the ensemble mean of all individual initializations from the respective reporting centers. This setup is inspired by three main ideas. Firstly, an established principle in forecasting asserts that a forecast is incomplete without an accompanying assessment of its skill. This idea comes from Henk Tennekes, who was a Dutch meteorologist. It underpinned the concept of forecast accuracy discussed by (Kalnay & Dalcher, 1987). Moreover, the growing literature describes the practice of combining forecasts, and their ensemble improves the accuracy of the forecast (Sheikh & Coulibaly, 2024). Furthermore, Furthermore, recent advancements in applied machine learning have shown promise in enhancing seasonal forecast performance. This is evident in hybrid seasonal forecasting, which combines dynamical ensemble outputs with machine learning to enhance accuracy and reliability (Ahmadi, Aminnejad, & Sabatsany, 2023; He, Li, DelSole, Ravikumar, & Banerjee, 2021; Qian, Jia, Lin, & Zhang, 2021).

3.2 Methods

Let X be a rectangular matrix of shape (n, d) where n is the number of grid points and d is the number of predictors. Let y be a vector of shape $(n, 1)$ that has the target precipitation values. Let w be a vector of shape $(d, 1)$ containing the weights of the individual features in X. In this case, X is the matrix of various GCMs described in Table 1, while y is the vector for GPCC containing the observed precipitation values.

3.2.1 Regression Methods

- **Linear Regression (LR)**

  Linear regression, introduced in the early 19th century through the least squares method and first applied to astronomical problems, became a fundamental tool in statistical modeling due to its interpretability and the computational challenges of non-linear modeling. It predicts quantitative outcomes by capturing the linear relationship between predictors and a response variable (James, Witten, Hastie, & Tibshirani, 2013). In ordinary least-squares linear regression, we find the value of w that minimizes the following term:

$$\min \|Xw - y\|^2 \tag{1}$$

  The goal of linear regression is to minimize the squared difference between the predictions of the linear model (Xw) and the truth (y). The prediction Xw is obtained by multiplying each predictor by its associated weight and summing of these products. The assumptions and derivations of the solution to this method are the basis of these formulations (Huang, 2018).

- **Ridge Regression (RidgeR): (L2 Regularization)**

  Ridge regression is a linear regression method that mitigates multicollinearity of predictive feature by adding an L2 penalty to shrink the coefficients of correlated predictors (Dar, Chand, Shabbir, & Kibria, 2023; Dar et al., 2023). As seen in Equation (1), with large weights, a small change in one of the predictors will lead to a large change in the forecast. Therefore, we amend linear regression to penalize large weights:

$$\min_w \|Xw - y\|_2^2 + \alpha\|w\|_2^2 \tag{2}$$

  The term $\alpha > 0$ is a regularization parameter. This regularized form of linear regression is often used to prevent overfitting with additional advantages such as numerical stability, and model complexity control power (Hoerl & Kennard, 1970).

- **Lasso Regression (L1 Regularization)**

  Lasso regression excels in handling high-dimensional datasets and performing feature selection, making it a fundamental method in supervised learning for regression modeling (Y. Wang, Zou, Xu, Xu, & Tang, 2025). It is an alternative to ridge regression introduced in Equation (2), which applies L1 regularization instead of L2:

$$\min_{w} \|Xw - y\|_2^2 + \lambda \|w\|_1 \tag{3}$$

where $\lambda > 0$ is the regularization parameter and $\|w\|_1$ is the L1 norm of the weight vector. Lasso regression encourages sparsity, which means that some of the weights may become exactly zero, leading to feature selection. Unlike ridge regression, Lasso regression is sparse which has additional benefit in terms of computational efficiency, interpretability and model generalization (Tibshirani, 1996).

- **Decision Tree Regression (DT)**

Decision tree regression is a non-linear supervised method that predicts continuous targets by partitioning the feature space, and it captures complex relationships without assuming any specific data distribution while remaining highly interpretable (Blockeel, Devos, Frénay, Nanfack, & Nijssen, 2023; Mienye & Jere, 2024). Given a data set $\{(x_i, y_i)\}_{i=1}^n$, the decision tree splits the data to minimize variance within each region Breiman, Friedman, Olshen, and Stone (2017). The regression estimator is as follows:

$$\hat{f}(X) = \hat{y} = \left(\frac{1}{n} \sum_{i=1}^{n} y_i \right) I_R(X) \tag{4}$$

where R is the sample space (the region containing all input feature vectors X) and $I_R(X)$ is the indicator function for the region R, which equals 1 if $X \in R$ and 0 otherwise. This means that within the region R, we approximate the response by the average of all y_i values whose corresponding inputs fall within R. Initially, R is the entire input space, which we assume to be a rectangular region in the feature space. If X_i is a continuous variable, we choose a real number a as a threshold value and divide R into two subregions:

$$R_1 = \{x \in R : x_j \leq a\}, \quad R_2 = \{x \in R : x_j > a\} \tag{5}$$

In this case, R_1 consists of all input vectors for which the value of the $i-th$ feature is less than or equal to a, and R_2 consists of those for which it is greater than a. This splitting process is repeated recursively to grow the tree, with the goal of minimizing the prediction error.

The division of R into R_1 and R_2 is chosen so that the sum of squared residuals of the estimator $\hat{f}$ is minimized. The sum of squared residuals to be minimized is defined below.

$$\sum_{i=1}^{n} \left(y_i - \hat{f}(X_i) \right)^2 \tag{6}$$

Stopping criteria include maximum depth and minimum samples per region, while pruning helps prevent overfitting (Miftachov & Reiß, 2025).

- **Random Forest Regression (RF)**

The Random Forests algorithm is an ensemble learning method that constructs multiple decision trees to enhance predictive accuracy and control overfitting and

amplify the importance of features (Breiman, 2001; Cutler, Cutler, & Stevens, 2012). Random forest regression combines predictions in trees formulated in Equation (4):

$$\hat{y} = \frac{1}{T}\sum_{t=1}^{T} f_t(X) \tag{7}$$

where T is the number of trees and $f_t(X)$ is the prediction of each tree in the forest.

- **Support Vector Regression (SVR)**

SVR is a regression technique that is based on a constrained optimization problem. It minimizes the complexity of the model while tolerating small deviations within the tolerance margin ϵ of the actual values. This ϵ is an insensitive loss function. The optimization process disregards errors that fall within the margin of ϵ (Vapnik, Golowich, & Smola, 1996). The optimization problem is given below:

$$\min_{w,b,\xi_i,\xi_i^*} \frac{1}{2}||w||^2 + C\sum_{i=1}^{N}(\xi_i + \xi_i^*) \tag{8}$$

subject to:

$$\begin{aligned} y_i - (w^T\phi(x_i) + b) &\leq \epsilon + \xi_i \\ (w^T\phi(x_i) + b) - y_i &\leq \epsilon + \xi_i^* \\ \xi_i, \xi_i^* &\geq 0, \quad i = 1, \ldots, N \end{aligned}$$

Where $\phi(x_i)$ is a mapping to a high dimensional space, w is the weight vector, b is the bias term, ξ_i, ξ_i^* are slack variables that allow deviations beyond ϵ while C is a regularization parameter.

- **XGBoost Regression (XGBR)**

XGBoost is a tree ensemble model with regularization mechanisms. It can effectively maximize and sparsify data sets by determining optimal default paths (Chen & Guestrin, 2016). The following is the objective function:

$$\mathcal{L}(\theta) = \sum_{i=1}^{n} l(y_i, \hat{y}_i) + \sum_{k} \Omega(f_k) \tag{9}$$

where $l(y_i, \hat{y}_i)$ is a loss function and $\Omega(f_k)$ is a regularization term for the complexity of the tree. This regularization term can be written in detail in the following relation.

$$\Omega(f) = \gamma T + \frac{1}{2}\lambda\|w\|_2^2$$

where T is the number of leaves, γ controls the complexity of the tree, λ is an L2 regularization parameter.

- **K-Nearest Neighbors Regression (KNN)**

KNN regression predicts the target value based on the average of the nearest neighbors k in the feature space using a distance function. The distance function and weighting methods may differ and lead to a different effectiveness (Cheng & Lin, 1981; Watson, 1964). In traditional K-Nearest Neighbors (KNN) regression, all K nearest neighbors have an equal influence on the predicted value. However, closer neighbors typically offer more valuable information. Distance-weighted KNN regression improves this approach by giving greater weight to nearer neighbors, making predictions more accurate. In the following formulation, we define distance-weighted KNN using inverse distance weighting (IDW). The predicted value $\hat{y}$ is given by:

$$\hat{y} = \frac{\sum_{x_i \in N_K(x)} w_i y_i}{\sum_{x_i \in N_K(x)} w_i} \tag{10}$$

where $N_K(x)$ is a set of K closest neighbors of x, w_i is the weight assigned to neighbor x_i, y_i is the observed value for neighbor x_i. These assigned weights can be generalized in the following equation:

$$w_i = \frac{1}{(d(x, x_i) + \epsilon)^p}$$

where $d(x, x_i)$ is the distance between x and x_i, ϵ is a small positive constant to avoid division by zero, and p is a power parameter that controls how rapidly weights decay with distance. If $p = 0$, the method reduces to simple averaging (standard KNN regression), $p = 1$, we obtain a standard inverse distance weighting, while $p > 1$, weights decay more quickly, emphasizing only very close neighbors.

- **Long Short-Term Memory (LSTM)**

Given that seasonal rainfall forecasts are sequential data, LSTM handles long-range time series data by using memory structures to manage extended information and solve nonlinear time series problems (Xhabafti, Vika, & Sinaj, 2024). The advantage of LSTM is the memory cell which helps to overcome the problem of vanishing gradients by allowing important data to persist over multiple time steps (Hochreiter & Schmidhuber, 1997; Noh, 2021). To define how this memory cell works leading to the formation of LSTM, the cell is obtained after defining the input gate, the forget gate, and the output gate. The work in (Van Houdt, Mosquera, & Nápoles, 2020) derives the LSTM and how it can be trained. It assumes a network made up of N processing blocks and M inputs with two activation functions, such as the sigmoid and hyperbolic functions. The sigmoid activation function is defined below:

$$\sigma(x) = \frac{1}{1 + e^{1-x}} \tag{11}$$

The hyperbolic tangent function is used as the block input and output activation function:

$$g(x) = \tanh(x) \tag{12}$$

The forward pass in this recurrent neural system is described below.

1. **Block input**: We start from this step. The input component of the block, which combines the current input $x^{(t)}$ and the output of this LSTM unit $y^{(t-1)}$ in the last iteration:
$$z^{(t)} = g(W_z x^{(t)} + R_z y^{(t-1)} + b_z) \tag{13}$$
where W_z and R_z are the weights associated with $x^{(t)}$ and $y^{(t-1)}$, respectively, while b_z stands for the bias weight vector.
2. **Input gate:** In this step, we update the input gate that combines the current input $x^{(t)}$, the output of the LSTM unit $y^{(t-1)}$, and the cell value $c^{(t-1)}$ in the last iteration. The following equation represents this procedure:
$$i^{(t)} = \sigma(W_i x^{(t)} + R_i y^{(t-1)} + p_i \odot c^{(t-1)} + b_i) \tag{14}$$
where $\odot$ denotes point-wise multiplication of two vectors, and W_i, R_i, and p_i are the weights associated with $x^{(t)}$, $y^{(t-1)}$, and $c^{(t-1)}$, respectively, while b_i represents the bias vector associated with this component.
In the previous steps, the LSTM layer determines which information should be retained in the cell states of the network $c^{(t)}$. This includes selecting the candidate values $z^{(t)}$ that could potentially be added to the cell states and the activation values $i^{(t)}$ of the input gates.
3. **Forget gate:** In this step, the LSTM unit determines which information should be removed from its previous cell states $c^{(t-1)}$. The activation values $f^{(t)}$ of the forget gates at time step t are calculated based on the current input $x^{(t)}$, the outputs $y^{(t-1)}$, and the state $c^{(t-1)}$ of the memory cells at the previous time step $(t-1)$, along with the peephole connections and the bias terms b_f of the forget gates. This is illustrated below:
$$f^{(t)} = \sigma(W_f x^{(t)} + R_f y^{(t-1)} + p_f \odot c^{(t-1)} + b_f) \tag{15}$$
where W_f, R_f, and p_f are the weights for $x^{(t)}$, $y^{(t-1)}$, and $c^{(t-1)}$, respectively, while b_f is bias weight vector.
4. **Memory Cell:** This step calculates the cell value by integrating the input of the block $z^{(t)}$, the input gate $i^{(t)}$, and the values of the forget gate, along with the value of the previous cell. The computation is shown below:
$$c^{(t)} = z^{(t)} \odot i^{(t)} + c^{(t-1)} \odot f^{(t)} \tag{16}$$
where $z^{(t)}$ is the block input, $i^{(t)}$ is the input gate, and $f^{(t)}$ is the forget gate.
5. **Output gate:** This is determined by combining the current input $x^{(t)}$, the previous LSTM output $y^{(t-1)}$ and the cell value from the last iteration $c^{(t-1)}$. It is described below:
$$o^{(t)} = \sigma(W_o x^{(t)} + R_o y^{(t-1)} + p_o \odot c^{(t)} + b_o) \tag{17}$$
where W_o, R_o, and p_o are the weights associated with $x^{(t)}$, $y^{(t-1)}$, and $c^{(t)}$, respectively, while b_o denotes the bias weight vector.

6. **Block output:** It is finally computed by combining values of the current cell $c^{(t)}$ with the current output gate $o^{(t)}$:

$$y^{(t)} = g(c^{(t)}) \odot o^{(t)} \tag{18}$$

where $g(c^{(t)})$ is the activation function applied to the cell state.

- **Bidirectional LSTM (BiLSTM)**

According to (Fan, Tang, Guo, & Wei, 2024; Hoseini & Notash, 2025), bidirectional Long Short-Term Memory (BiLSTM) networks are deep learning architectures that extend traditional LSTMs by processing data in both forward and backward directions, capturing contextual information from past and future time steps. This bidirectional processing improves the model's ability to understand complex temporal patterns, making BiLSTMs particularly effective for time series forecasting. The flowchart and equations for standard LSTM, based on the forward pass of information, have been established. Building on this, BiLSTM processes sequences in both forward and backward directions, capturing dependencies from past and future inputs. The work of (Schuster & Paliwal, 1997) illustrated the mathematical derivations underlying BiLSTM, providing a formal representation of this bidirectional information flow.

1. **Forward LSTM (Processing from 1 to N):**

$$\begin{aligned}
\overrightarrow{z^{(t)}} &= \tanh(W_z x^{(t)} + R_z \overrightarrow{y^{(t-1)}} + b_z) \\
\overrightarrow{i^{(t)}} &= \sigma(W_i x^{(t)} + R_i \overrightarrow{y^{(t-1)}} + p_i \odot \overrightarrow{c^{(t-1)}} + b_i) \\
\overrightarrow{f^{(t)}} &= \sigma(W_f x^{(t)} + R_f \overrightarrow{y^{(t-1)}} + p_f \odot \overrightarrow{c^{(t-1)}} + b_f) \\
\overrightarrow{c^{(t)}} &= \overrightarrow{z^{(t)}} \odot \overrightarrow{i^{(t)}} + \overrightarrow{c^{(t-1)}} \odot \overrightarrow{f^{(t)}} \\
\overrightarrow{o^{(t)}} &= \sigma(W_o x^{(t)} + R_o \overrightarrow{y^{(t-1)}} + p_o \odot \overrightarrow{c^{(t)}} + b_o) \\
\overrightarrow{y^{(t)}} &= \tanh(\overrightarrow{c^{(t)}}) \odot \overrightarrow{o^{(t)}}
\end{aligned} \tag{19}$$

2. **Backward LSTM (Processing from N to 1):**

$$\begin{aligned}
\overleftarrow{z^{(t)}} &= \tanh(W_z x^{(t)} + R_z \overleftarrow{y^{(t+1)}} + b_z) \\
\overleftarrow{i^{(t)}} &= \sigma(W_i x^{(t)} + R_i \overleftarrow{y^{(t+1)}} + p_i \odot \overleftarrow{c^{(t+1)}} + b_i) \\
\overleftarrow{f^{(t)}} &= \sigma(W_f x^{(t)} + R_f \overleftarrow{y^{(t+1)}} + p_f \odot \overleftarrow{c^{(t+1)}} + b_f) \\
\overleftarrow{c^{(t)}} &= \overrightarrow{z^{(t)}} \odot \overleftarrow{i^{(t)}} + \overleftarrow{c^{(t+1)}} \odot \overleftarrow{f^{(t)}} \\
\overleftarrow{o^{(t)}} &= \sigma(W_o x^{(t)} + R_o \overleftarrow{y^{(t+1)}} + p_o \odot \overleftarrow{c^{(t)}} + b_o)
\end{aligned}$$

$$\overleftarrow{y^{(t)}} = \tanh\left(\overleftarrow{c^{(t)}}\right) \odot \overleftarrow{o^{(t)}} \tag{20}$$

3. **Final BiLSTM Output:**

The output at each time step t is the concatenation of forward and backward hidden states. This is given by the following relation, where $\oplus$ denotes the concatenation of the outputs in Equations 19 and 20.

$$y^{(t)} = \overrightarrow{y^{(t)}} \oplus \overleftarrow{y^{(t)}} \tag{21}$$

- **Kolmogorov-Arnold Networks (KAN)**

Kolmogorov-Arnold networks (KAN) are a type of neural network based on the Kolmogorov-Arnold representation theorem, which states that any multivariate continuous function can be written as the sum of continuous functions of a single variable. This concept was developed by Andrey Kolmogorov and Vladimir Arnold. Unlike MLPs, which use fixed activation functions at the nodes (neurons), KANs apply learnable activation functions to the edges (weights) (Z. Liu et al., 2024). These are learnable spline-based functions instead of fixed activation functions. This approach enables more flexible and interpretable representations of high-dimensional functions (Somvanshi, Javed, Islam, Pandit, & Das, 2024). The KAN foundation theorem states that any continuous multivariable function can be expressed as a finite superposition of continuous univariate functions $f(x_1, x_2, x_3, \ldots, x_n)$. The mathematical formulation is described below.

$$f(x_1, x_2, x_3, \ldots, x_n) = \sum_{q=1}^{2n+1} \phi_q \left(\sum_{p=1}^{n} \varphi_{q,p}(x_p) \right) \tag{22}$$

where $\phi_q : \mathbb{R} \to \mathbb{R}$ and $\varphi_{q,p} : [0,1] \to \mathbb{R}$ are continuous univariate functions, the inner sum $\sum_{p=1}^{n} \varphi_{q,p}(x_p)$ represents the transformation of individual input variables x_p through the function $\varphi_{q,p}$, which maps each x_p into a new space, and the outer sum $\sum_{q=1}^{2n+1} \phi_q$ then combines these transformed inputs to approximate the target function $f(x_1, x_2, \ldots, x_n)$.

3.2.2 Metrics

- **Bias and Explainable Variability**

There are various evaluation metrics for regression tasks. In this study, we are using bias quantification metrics such as the root mean squared error (RMSE) and mean absolute error (MAE). On the other hand, we quantified the goodness of fit using the determination coefficient R^2, which indicates how much of the variation in the dependent variable can be explained by the independent variables (Chicco, Warrens,

& Jurman, 2021).

$$RMSE = \sqrt{\frac{1}{N}\sum_{i=1}^{N}(y_i - \hat{y}_i)^2} \tag{23}$$

$$MAE = \frac{1}{N}\sum_{i=1}^{N}|y_i - \hat{y}_i| \tag{24}$$

$$R^2 = 1 - \frac{\sum_{i=1}^{N}(y_i - \hat{y}_i)^2}{\sum_{i=1}^{N}(y_i - \bar{y})^2} \tag{25}$$

From equations (23), (24) and (25), y_i represents the actual values; $\hat{y}_i$ for the predicted values; $\bar{y}$ for the mean of the actual values; while N is the number of observations.

- **Feature Importance**

  In this study, we are using values of **SHAP** (SHapley Additive exPlanations). SHAP assigns each characteristic an importance value for a particular prediction to measure the importance of specific features in observed predictions for local and global attributions. This method is an unbiased method to estimate the importance of features in regression and classification tasks (Lundberg & Lee, 2017). This method requires retraining the model on all subsets of features $S \subseteq F$, where F represents the entire set of features. The importance assigned to each feature reflects its effect on the prediction of the model. If $f_{S\cup\{i\}}$ is a model that includes the feature and f_S is a model that excludes the feature, the contribution of the feature i is computed as:

$$f_{S\cup\{i\}}(x_{S\cup\{i\}}) - f_S(x_S) \tag{26}$$

where x_S represents the values of the features in S. Since this effect depends on interactions with other features, it is calculated for all possible subsets $S \subseteq F \setminus \{i\}$. We are using mean absolute **SHAP** values to quantify the importance of global features. Shapley values are computed as a weighted average of all possible contributions:

$$\phi_i = \sum_{S\subseteq F\setminus\{i\}} \frac{|S|!(|F| - |S| - 1)!}{|F|!}\left[f_{S\cup\{i\}}(x_{S\cup\{i\}}) - f_S(x_S)\right] \tag{27}$$

This formulation ensures a fair distribution of the importance of features by considering all possible feature interactions (Anoyege & Alatinga, 2024)

4 Results and Discussion

4.1 Bias and Explainable Variability in Classical Machine Learning Algorithms

This section presents the evaluation of linear and nonlinear models for seasonal rainfall prediction.

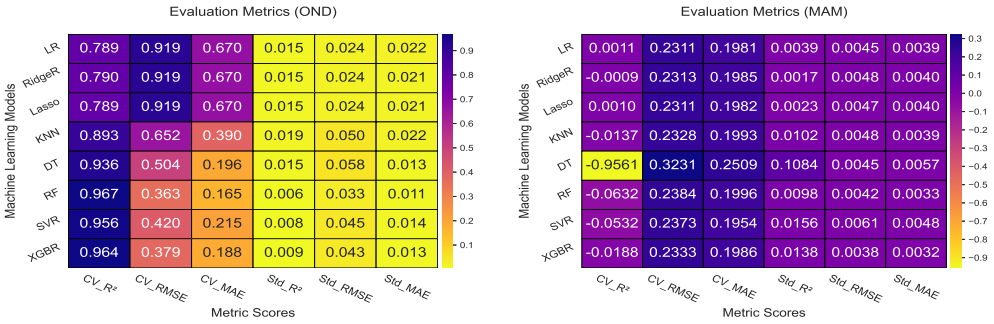

(a) (b)

Fig. 4: RMSE, MAE, R^2, and deviations for OND (a) and MAM (b) seasons.

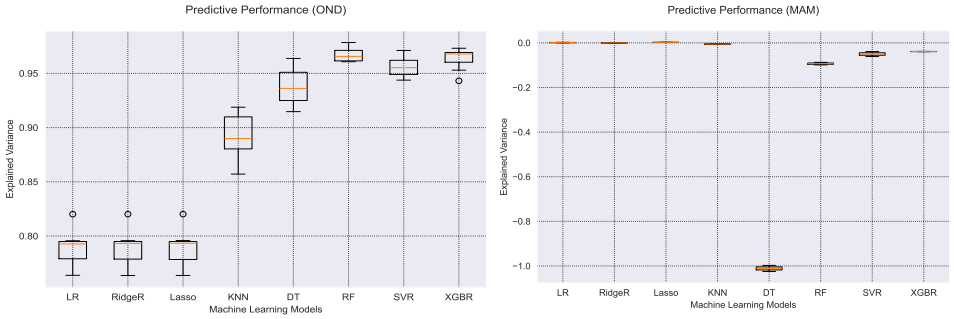

(a) (b)

Fig. 5: Goodness of fit comparison for the OND and the MAM seasons across machine learning algorithms

Figures 4 and 5 show the results of the three linear models, such as linear regression (LR) and its two regularized extensions, which penalize the model for learning the large feature weights. These models scored similarly in terms of bias and coefficient of determination (R^2). We also deployed nonlinear models on the data set, and

results are reported in a contrasting manner for the seasons. Nonlinear models outperformed linear models during the OND season, attaining a goodness of fit above 89%. Among these, the random forest model achieved the highest performance, with a 96.7% mean cross-validated explainable variability over 10 folds and the lowest error metrics (RMSE and MAE). These results highlight the superiority of nonlinear approaches for OND season prediction. The values in CV_RMSE & CV_MAE represent cross-validated $RMSE$ and MAE. Moreover, std_RMSE, std_MAE, and std_R^2, represent the standard deviations of mean cross-validated RMSE, MAE, and $\mathbf{R^2}$, respectively.

In contrast, both models performed poorly on MAM season, but linear were slightly better. These results suggest that classical machine learning algorithms can perform well during the OND season but struggle when applied to the data for the MAM season. This highlights the complexity of modeling rainfall during the MAM season in the region.

4.2 Sample Predictions of Random Forest and Their Feature Importance Compared to Linear Model Weights (OND)

The Random Forest outperformed other traditional machine learning algorithms in predicting the seasonal rainfall of OND. The results presented in Figure 6 describe the learnable weights of the features in multiple regression tasks. Fortunately, the importance of each feature in random forests is amplified, which is not the case for linear models. In both linear and ridge regression, half of the features exhibited negative coefficients, while the remaining half had positive coefficients. In contrast, Lasso regression identified only four weighted features, three with positive coefficients and one with a negative coefficient. The results of Lasso stressed the feature selection capability as discussed by (Heilemann et al., 2024; Song & Zhang, 2024).

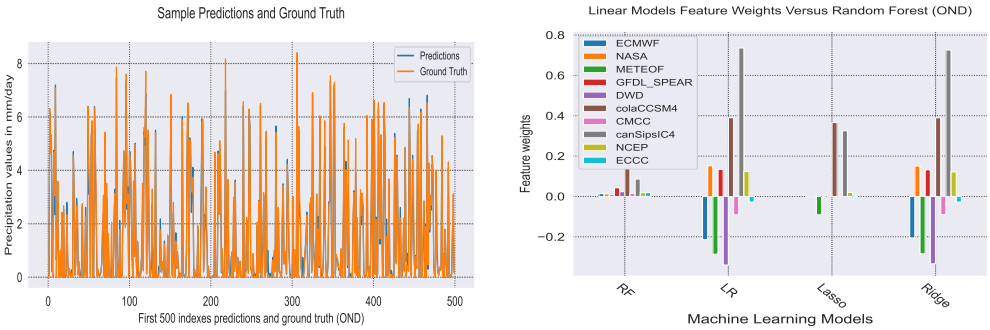

(a) (b)

Fig. 6: Random Forest predictions for OND (a) with feature importance, and linear model predictions (b) with feature weights.

Irrespective of the specific variant, linear models consistently allocate larger absolute weights to predictors compared to tree-based models, such as random forest, and

this disparity is rooted in the underlying mathematical structure of linear estimators, including Lasso and ridge regression. These formulations introduce regularization terms to penalize large feature weights, thereby constraining the model and improving generalization while reducing overfitting. These weights do not necessarily indicate feature importance. Feature importance is assessed by generating predictions excluding the target feature and evaluating its attribution through all possible global interactions involving that feature.

4.3 Feature Importance

The contribution of features to prediction is season-specific. Figure 7 displays the importance of features, calculated using mean absolute **SHAP** values. For the OND season, the feature importance magnitudes are high overall, reflecting the substantial weights contributing to the model predictions.

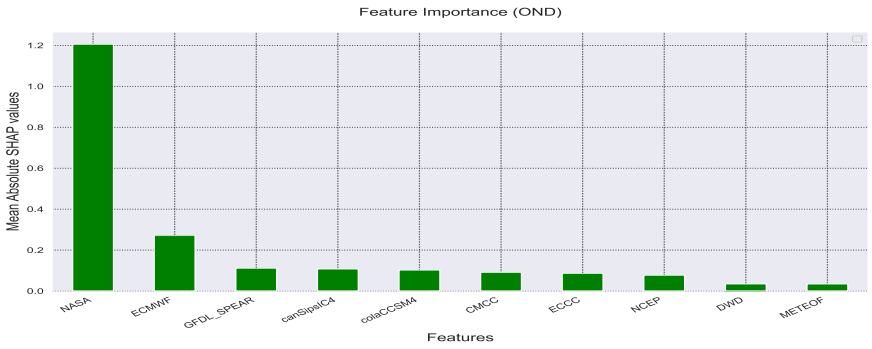

(a)

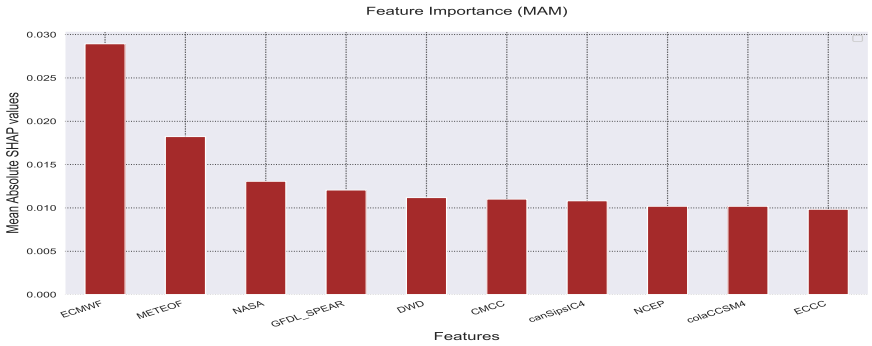

(b)

Fig. 7: Feature importance for OND (a) and MAM (b)

Given that the features are ordered in descending order of importance, NASA is the best predictor of the region among the global circulation models (GCMs) considered for OND. Moreover, ECMWF is the major contributing feature in the model

predictions for MAM. The least contributing feature for the OND season is Météo France, whereas for the MAM season, it is ECCC. The level of explainability influences the mean absolute SHAP values since the importance in OND is of a higher amplitude compared to that of the MAM season. This is evident, as classical machine learning algorithms performed poorly on the MAM season during this experiment. In summary, ECMWF and NASA consistently appear among the top three contributing features in predictions regardless of the season. Furthermore, ECCC, NCEP, and DWD consistently rank among the four least contributing features across all seasons.

4.4 Features Percentage Contribution in Predicted Values

The contribution of GCMs varies with the seasons. Figure 8 shows the percentage contributions for OND (a) and MAM (b), respectively. These results describe the situation of simulating various precipitations over time. The fact that the GCM is critically dominant in one season does not necessarily mean that it will hold this record for the other seasons.

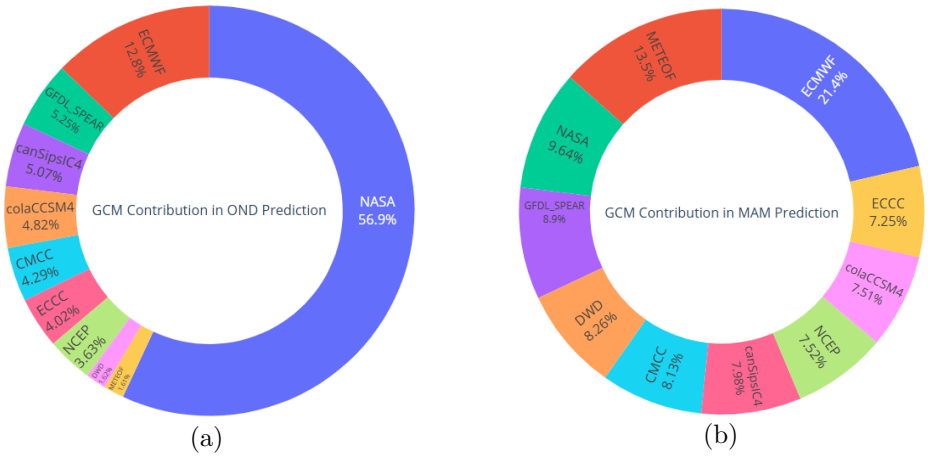

(a) (b)

Fig. 8: Feature percentage contributions for OND (a) and MAM (b).

The percentage contribution across the seasons is compared, and the results show that NASA has taken a lead of about 56.9%, which is greater than the remaining portions of the 9 GCMs considered in MAM. This is not closer to an even contribution of individual predictors. In contrast, ECMWF is the leading GCM for OND, accounting for 21.4% of the total contribution, while the remaining nine GCMs share the other 78.6%. This distribution crucially highlights the close agreement among GCMs used for the OND season in predicting observed rainfall over GHA. It underscores the value of multi-model ensemble approaches in capturing regional precipitation patterns accurately.

ECMWF, NASA, Météo France, and GFDL_SPEAR account for over 53.44% of the total percentage contributions in MAM. In OND, ECMWF, NASA, CanSipsIC4, and

GFDL_SPEAR together contribute 80.02%. ECMWF and NASA consistently appear among the top three performing GCMs across the seasons.

4.5 Bias and Explainable Variability in Deployed Deep Learning Architectures

The predictions of deep learning models are season-specific. Figure 9 shows the level of biases and explained variability in the training of LSTM, BiLSTM, and KAN in the OND and MAM seasons. We trained a one-layer model LSTM on unscaled data (1L_Unscaled_LSTM), and the rest of the architectures were all trained on scaled data.

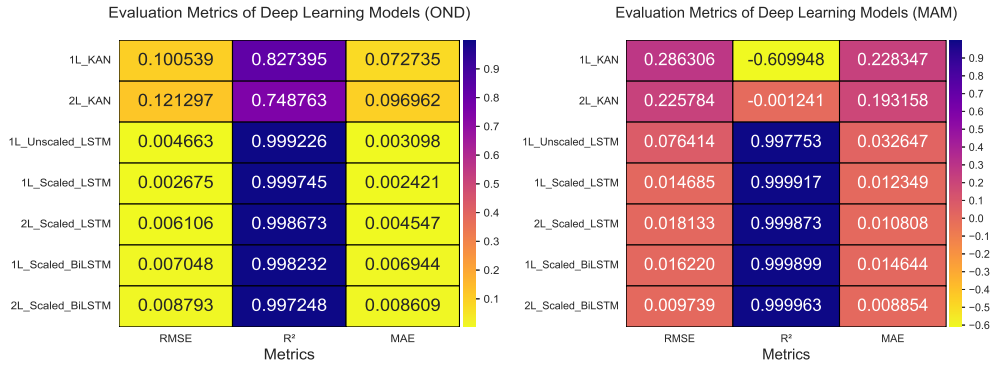

(a) (b)

Fig. 9: Comparison of RMSE, MAE, and R^2 for deep learning architectures in OND (a) and MAM (b).

The performance of LSTM architectures is excellent in both seasons. The best architecture for OND is the 1L_Scaled_LSTM, a model with one hidden layer trained on scaled data, achieving a coefficient of determination of 99.97%, an MAE of 0.0024, and an RMSE of 0.0026. It is worth noting that the scaler that maps data values between 0 and 1 for faster computations is used. On the other hand, the MAM season is well predicted with a two-layer bidirectional LSTM on scaled data (2L_Scaled_BiLSTM) with 99.9963% of explainable variability, 0.0097 RMSE, and 0.0088 MAE.

The MAM season demonstrates persistent predictive challenges, as both KAN architectures struggled to produce accurate predictions. We may attribute the good performance of the LSTM models to the fact that there is a memory cell in them. It retains the historical dependencies within the prediction process. This capability is absent in classical machine learning algorithms and some deep learning architectures, such as a simple KAN.

4.6 Selection of the Best Model Based on its Predictive Performance

This section presents the criteria and evaluation of deep learning architectures for seasonal rainfall prediction. The models were assessed based on explainable variability and bias metrics, including RMSE and MAE.

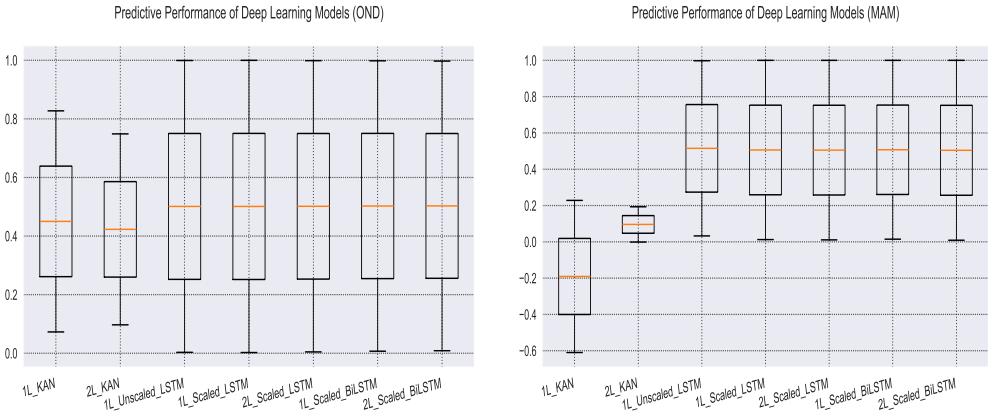

(a) (b)

Fig. 10: Goodness of fit for OND (a) and MAM (b) across different deep learning architectures.

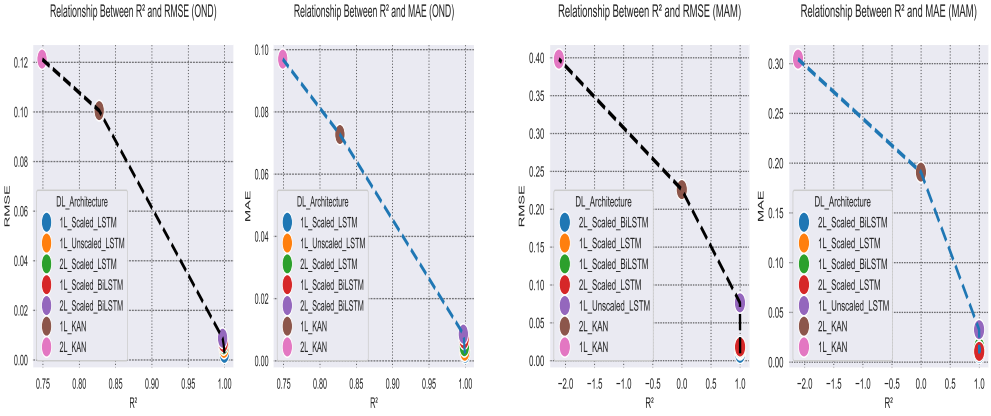

(a) (b)

Fig. 11: Bias–variance relationships for the OND (a) and MAM (b) seasons across deep learning architectures.

Figures 10 and 11 illustrate the criteria used to select the best prediction model. We wanted to have a machine learning or deep learning architecture that has a high level of explainable variability and a very low level of bias quantification metrics in terms of root mean squared error (RMSE) and mean absolute error (MAE). We compared all of the algorithms deployed to find that the higher the bias, the lower the coefficient of determination, and the converse is also true. The performance of deep learning architectures is significantly positive in the OND season. Moreover, the depth of the neural network is shallow to achieve better predictions. In most cases, a single-layer network demonstrated superior performance compared to two-hidden-layer architectures employing multilayer perceptron-based models, including BiLSTM. The same is true for the deep learning architecture that had trainable functions at the edges, which is KAN. This implies that the function that models the OND precipitation forecasts has a low complexity. On the other hand, the MAM season was very complex to model using GCMs as features of prediction in either classical machine learning algorithms or KAN. Better predictions can only be achieved by using deep learning architectures with the memory cell, such as LSTM and BiLSTM.

It is worth noting that the best prediction architecture is the BiLSTM two-layer architecture, implying that BiLSTM architectures achieved better performance by adding the new hidden layer (deeper training).

On the other hand, one-layer LSTM was the second-best predicting architecture. This shows the difference in perception of thinking that deeper training may lead to better prediction. It demonstrates how architecture-specific it is.

In fact, these are inherent characteristics of functions exhibiting high complexity in modeling tasks. Predicting MAM rainfall is likely to incur substantial biases when based solely on prediction features such as GCMs, particularly when employing traditional machine learning models. These results also provide more details on the relationship between bias and explainable variability in the search for a better prediction architecture. There is an inverse relationship between bias and explainable variability. In fact, the LSTM architecture's predictions show minimal variation across all considered seasons. Moreover, they consistently achieved the highest predictive performance across all seasons, positioning them as the preferred models for accurate seasonal forecasting in the region. This level of low variance in errors is essential for informing agricultural decision-making and optimizing practices.

4.7 Trainability of the Best Model and Effect of Extending the Forecasting Window

Training and test loss curves are season-specific, and we trained different models to determine that deep learning architectures yield the best results. Moreover, the performance of these architectures is also season-specific, highlighting the importance of tailoring model selection to each seasonal dataset.

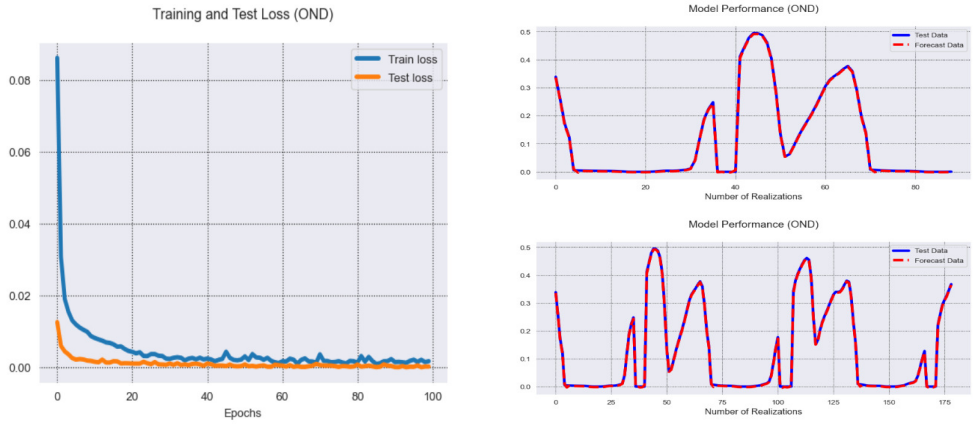

(a) (b)

Fig. 12: Panel (a): training/test loss; panel (b): OND forecast (1L_Scaled_LSTM) model.

Figures 12 and 13 display the training and testing loss curves over 100 training epochs. Moreover, the right-hand side of the figures gives more details about the forecasting window elongation on top-performing architectures. The OND model's test loss indicates an almost perfect mapping, with a maximum value below 0.02. However, such a low value may indicate overfitting. This is supported by the observation that the test loss curve starts at a point not aligned with the training loss curve.

When we extend the forecast window, it tends to produce near-perfect predictions but may be less practical due to fluctuations in atmospheric conditions that induce the water cycle and rainfall in particular. Furthermore, most agricultural activities occur during the rainy seasons, making accurate rainfall prediction especially important. The best predicting architecture for MAM is working better than the best predicting architecture for OND in terms of explainable variability.

The training and test losses for MAM follow almost the same pattern, which indicates a good generalization ability. The act of extending the forecasting window tends to produce perfect predictions, and the model is relatively stable in explainable variability with a very small change in bias metric scores. In fact, the best architecture for OND is too fast to generalize, whereas the best architecture for MAM takes time to generalize.

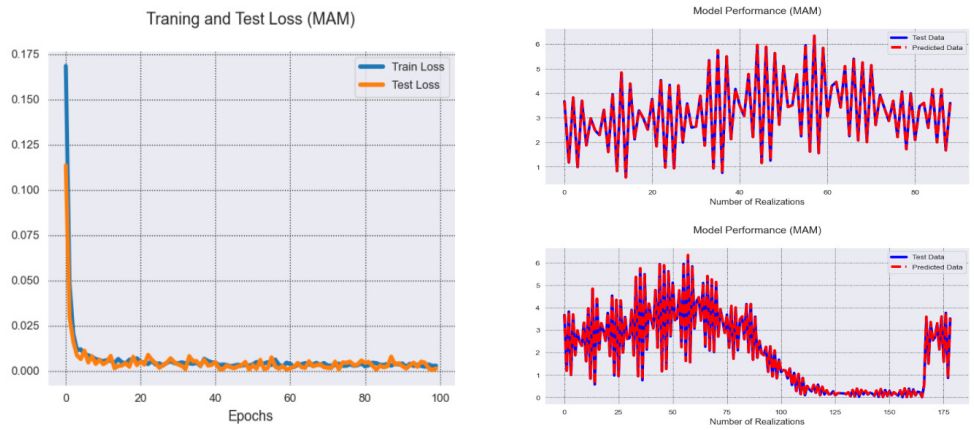

(a) (b)

Fig. 13: Panel (a): training/test loss; panel (b): MAM forecast (2L_Scaled_BiLSTM) model.

5 Conclusion and Recommendations

5.1 Conclusion

We started this study with the specific goal of identifying the performance of global climate models (GCMs) in simulating the seasonal rainfall forecast in the Greater Horn of Africa (GHA). The main idea was to evaluate the performance of GCMs on short and long rains with critical interest in long rains because of the low skill of seasonal forecasts in this season of MAM. To do so, we began with the season that exhibits higher forecast skill in the region: OND ("short rains"). The results of the deployed methods indicate the potential for accurate predictions during the OND season. This is particularly evident when applying classical machine learning algorithms. Among these, tree-based approaches, such as decision trees and random forests, demonstrate strong predictive performance. Moreover, methods such as support vector regression and XGBoost are also serving the good purpose of this task.

The best classical machine learning algorithm was the random forest, with a very small difference from the predictions of XGBoost. Since this season was somehow easy to predict by classical machine learning algorithms, deep learning architectures such as LSTM and BiLSTM outperformed them with a high level of explained variability and less prediction bias. The KAN model (1L_KAN) managed to outperform linear models. The best prediction model was found to be a one-layer LSTM on scaled data. This highlights that we do not need to increase the depth of deep learning architecture to have better predictions for OND. We can also highlight the top three contributing GCMs in predictions, such as NASA, ECMWF, and GFDL_SPEAR. On the other hand, classical machine learning algorithms performed poorly in the MAM rainfall seasonal forecasts of the region with an insignificant level of explainable variability. The KAN deep learning architecture also performed poorly in this case.

The only credible architectures to predict MAM seasonal rainfall from deployed models are memory cell-based architectures such as LSTM and BiLSTM. The findings suggest that training LSTM or BiLSTM architectures has the potential to enhance prediction accuracy. However, increasing the depth of these networks may introduce overfitting or instability, thereby reducing the robustness of predictions. This trade-off underscores the importance of optimizing network architecture to balance accuracy and generalization.

The best prediction architecture was found to be a two-layer BiLSTM on scaled data. We may also highlight the three main contributing features in a multi-model ensemble prediction for MAM, which are ECMWF, Météo France, and NASA.

This study builds on prior approaches that used the arithmetic mean of individual GCM outputs as predictors by advancing a more systematic framework for constructing multi-model ensemble predictions. It highlights that the predictive skill of a given algorithm is season-dependent, as methods that perform well in one season may not yield comparable accuracy in another. These variations are linked to the differing complexities of atmospheric and oceanic processes that drive rainfall variability across seasons in the Greater Horn of Africa.

Overall, the multi-model ensemble prediction methodology sustains the hybrid-based approach to seasonal rainfall forecasting, integrating diverse models to enhance predictive reliability. By combining multiple sources of information, it strengthens the accuracy and resilience of forecasts across varying climatic conditions. Consequently, this approach supports the principle that "forewarned is forearmed," providing valuable insights for informed agricultural planning and decision-making.

5.2 Recommendations

We used GCMs as predictive features for short and long rains. Fortunately, modeling OND was quite possible using both classical machine learning algorithms and deep learning architectures. Modeling rainfall forecasts for the MAM season proved highly challenging when using traditional machine learning algorithms. Therefore, deep learning architectures may offer a more effective alternative due to their ability to capture complex temporal dependencies. In particular, architectures with memory cells can retain the history of feature weights while propagating information through the network, thereby enhancing the representation of sequential patterns in the data. A limitation of this study is that we did not integrate additional regional and global climate drivers with GCM output. This integration may help assess whether classical machine learning algorithms can produce more reliable and robust predictions in regional rainfall forecasting, particularly for long rains.

Supplementary information

- **Acknowledgements** The authors acknowledge and thank the IGAD Climate Prediction and Applications Centre for their collaboration, without which this study would not have been possible.

- **Author Contributions** Conceptualization: A.H., M.B.S., P.N., M.G.; Methodology: A.H., M.B.S., P.N., M.G.; Formal analysis: A.H., M.B.S., P.N, M.G.; Data curation: A.H., M.B.S., P.N, M.G.; Writing—original draft: A.H.;Writing—review & editing: A.H., M.B.S., P.N, M.G., M.K, R.K.; Visualization: A.H., M.B.S., P.N, M.G.; Supervision: M.B.S., P.N., M.G., M.K., R.K.

- **Funding** This publication was made possible by a grant from Carnegie Corporation of New York (provided through the African Institute for Mathematical Sciences). The statements made and views expressed are solely the responsibility of the author(s).

- **Data Availability:** IRI Data Library precipitation data from this link and C3S data from here.

- **Code availability** Code is available on request.

Declarations

- **Competing interests** The authors declare no competing interests.

- **Ethics approval** Not applicable.

- **Consent to participate** Not applicable.

- **Consent for publication** Not applicable.

References

Agbasi, J.C., Egbueri, J.C., Ayejoto, D.A., Unigwe, C.O., Omeka, M.E., Nwazelibe, V.E., ... Fakoya, A.A. (2023). The impact of seasonal changes on the trends of physicochemical, heavy metal and microbial loads in water resources of southeastern nigeria: a critical review. *Climate change impacts on Nigeria: environment and sustainable development*, 505–539, https://doi.org/https://doi.org/10.1007/978-3-031-21007-5_25

Ahmadi, H., Aminnejad, B., Sabatsany, H. (2023). Application of machine learning ensemble models for rainfall prediction. *Acta Geophysica*, *71*(4), 1775–1786, https://doi.org/https://doi.org/10.1007/s11600-022-00952-y

Akbar, A.A., Darmawan, Y., Wibowo, A., Rahmat, H.K. (2024). Accuracy assessment of monthly rainfall predictions using seasonal arima

and long short-term memory (lstm). *Journal of Computer Science and Engineering (JCSE)*, *5*(2), 100–115, Retrieved from https://icsejournal.com/index.php/JCSE/article/download/843/216

Anoyege, R., & Alatinga, K.A. (2024). Impacts of illegal mining activities on water quality for irrigation and implications for public health: A case study of the oda river in the ashanti region of ghana. *Journal of Water and Health*, *22*(10), 1886–1898,

Antonio, B., McRae, A.T., MacLeod, D., Cooper, F.C., Marsham, J., Aitchison, L., ... Watson, P.A. (2025). Postprocessing east african rainfall forecasts using a generative machine learning model. *Journal of Advances in Modeling Earth Systems*, *17*(3), e2024MS004796, https://doi.org/https://doi.org/10.1029/2024MS004796

Anwar, M., Winarno, E., Hadikurniawati, W., Novita, M. (2021). Rainfall prediction using extreme gradient boosting. *Journal of physics: Conference series* (Vol. 1869, p. 012078).

Anyah, R.O., & Qiu, W. (2012). Characteristic 20th and 21st century precipitation and temperature patterns and changes over the greater horn of africa. *International Journal of Climatology*, *32*(3), 347–363, https://doi.org/https://doi.org/10.1002/joc.2270

Assamnew, A.D., & Tsidu, G.M. (2020). The performance of regional climate models driven by various general circulation models in reproducing observed rainfall over east africa. *Theoretical and Applied Climatology*, *142*, 1169–1189, https://doi.org/https://doi.org/10.1007/s00704-020-03357-3

Bacci, M., Idrissa, O., Zini, C., Burrone, S., Sitta, A.A., Tarchiani, V. (2023). Effectiveness of agrometeorological services for smallholder farmers: the case study in the regions of dosso and tillabéri in niger. *Climate Services*, *30*, 100360, https://doi.org/https://doi.org/10.1016/j.cliser.2023.100360

Bacci, M., Ousman Baoua, Y., Tarchiani, V. (2020). Agrometeorological forecast for smallholder farmers: A powerful tool for weather-informed crops management in the sahel. *Sustainability*, *12*(8), 3246, https://doi.org/https://doi.org/10.3390/su12083246

Barrera-Animas, A.Y., Oyedele, L.O., Bilal, M., Akinosho, T.D., Delgado, J.M.D., Akanbi, L.A. (2022). Rainfall prediction: A comparative analysis of modern machine learning algorithms for time-series forecasting. *Machine Learning with Applications*, *7*, 100204, https://doi.org/https://doi.org/10.1016/j.mlwa.2021.100204

Basha, C.Z., Bhavana, N., Bhavya, P., Sowmya, V. (2020). Rainfall prediction using machine learning & deep learning techniques. *2020 international conference on electronics and sustainable communication systems (icesc)* (pp. 92–97).

Basist, A., Bell, G.D., Meentemeyer, V. (1994). Statistical relationships between topography and precipitation patterns. *Journal of climate*, *7*(9), 1305–1315,

Becker, E., Kirtman, B.P., Pegion, K. (2020). Evolution of the north american multi-model ensemble. *Geophysical Research Letters*, *47*(9), e2020GL087408, https://doi.org/10.1029/2020GL087408 Retrieved from https://doi.org/10.1029/2020GL087408

Blockeel, H., Devos, L., Frénay, B., Nanfack, G., Nijssen, S. (2023). Decision trees: from efficient prediction to responsible ai. *Frontiers in artificial intelligence*, *6*, 1124553, https://doi.org/https://doi.org/10.3389/frai.2023.1124553

Bowden, J.H., & Semazzi, F.H. (2007). Empirical analysis of intraseasonal climate variability over the greater horn of africa. *Journal of Climate*, *20*(23), 5715–5731, https://doi.org/https://doi.org/10.1175/2007JCLI1587.1

Breiman, L. (2001). Random forests. *Machine learning*, *45*, 5–32, https://doi.org/https://doi.org/10.1023/A:1010933404324

Breiman, L., Friedman, J., Olshen, R.A., Stone, C.J. (2017). *Classification and regression trees*. Routledge.

Bruno Soares, M., Daly, M., Dessai, S. (2018). Assessing the value of seasonal climate forecasts for decision-making. *Wiley Interdisciplinary Reviews: Climate Change*, *9*(4), e523, https://doi.org/https://doi.org/10.1002/wcc.523

Calì Quaglia, F., Terzago, S., von Hardenberg, J. (2022). Temperature and precipitation seasonal forecasts over the mediterranean region: added value compared to simple forecasting methods. *Climate Dynamics*, *58*(7), 2167–2191, https://doi.org/https://doi.org/10.1007/s00382-021-05895-6

Camberlin, P., & Philippon, N. (2002). The east african march–may rainy season: Associated atmospheric dynamics and predictability over the 1968–97 period. *Journal of climate*, *15*(9), 1002–1019,

Chen, T., & Guestrin, C. (2016). Xgboost: A scalable tree boosting system. *Proceedings of the 22nd acm sigkdd international conference on knowledge discovery and data mining* (pp. 785–794).

Cheng, K.-F., & Lin, P.-E. (1981). Nonparametric estimation of a regression function. *Zeitschrift für Wahrscheinlichkeitstheorie und verwandte Gebiete*, *57*, 223–233, https://doi.org/https://doi.org/10.1007/BF00535491

Chicco, D., Warrens, M.J., Jurman, G. (2021). The coefficient of determination r-squared is more informative than smape, mae, mape, mse and rmse in regression analysis evaluation. *Peerj computer science*, *7*, e623, https://doi.org/https://doi.org/10.7717/peerj-cs.623

Cutler, A., Cutler, D.R., Stevens, J.R. (2012). Random forests. *Ensemble machine learning: Methods and applications*, 157–175, https://doi.org/https://doi.org/10.1007/978-1-4419-9326-7_5

Dar, I.S., Chand, S., Shabbir, M., Kibria, B.G. (2023). Condition-index based new ridge regression estimator for linear regression model with multicollinearity. *Kuwait Journal of Science*, *50*(2), 91–96, https://doi.org/https://doi.org/10.1016/j.kjs.2023.02.013

Daron, J., Michaelides, K., Hassaballah, K., Quichimbo, A., Parfitt, R., Stacey, J., ... Singer, M.B. (2025). Simbol: A method to co-produce impact-based seasonal outlooks. *Climate Services*, *38*, 100579, https://doi.org/https://doi.org/10.1016/j.cliser.2025.100579

Deman, V.M., Koppa, A., Waegeman, W., MacLeod, D.A., Bliss Singer, M., Miralles, D.G. (2022). Seasonal prediction of horn of africa long rains using machine learning: the pitfalls of preselecting correlated predictors. *Frontiers in Water*, *4*, 1053020, https://doi.org/https://doi.org/10.3389/frwa.2022.1053020

Devadarshini, E., Bhuvaneswari, K., Mohan Kumar, S., Geethalakshmi, V., Dhasarathan, M., Senthil, A., ... others (2024). Spatiotemporal performance

evaluation of high-resolution multiple satellite and reanalysis precipitation products over the semiarid region of india. *Environmental Monitoring and Assessment*, *196*(11), 1006, https://doi.org/https://doi.org/10.1007/s10661-024-13152-6

Dyer, E., & Washington, R. (2021). Kenyan long rains: A subseasonal approach to process-based diagnostics. *Journal of Climate*, *34*(9), 3311–3326, https://doi.org/https://doi.org/10.1175/JCLI-D-19-0914.1

Ehsan, M.A., Tippett, M.K., Robertson, A.W., Almazroui, M., Ismail, M., Dinku, T., ... Teshome, A. (2021). Seasonal predictability of ethiopian kiremt rainfall and forecast skill of ecmwf's seas5 model. *Climate Dynamics*, *57*(11), 3075–3091, https://doi.org/https://doi.org/10.1007/s00382-021-05855-0

Fan, Y., Tang, Q., Guo, Y., Wei, Y. (2024). Bilstm-mlam: a multi-scale time series prediction model for sensor data based on bi-lstm and local attention mechanisms. *Sensors*, *24*(12), 3962, https://doi.org/https://doi.org/10.3390/s24123962

Fuentes-Franco, R., Giorgi, F., Pavia, E.G., Graef, F., Coppola, E. (2018). Seasonal precipitation forecast over mexico based on a hybrid statistical–dynamical approach. *Int. J. Climatol*, *38*(11), 4051–4065, https://doi.org/10.1002/joc.5550

Funk, C., Harrison, L., Shukla, S., Pomposi, C., Galu, G., Korecha, D., ... others (2018). Examining the role of unusually warm indo-pacific sea-surface temperatures in recent african droughts. *Quarterly Journal of the Royal Meteorological Society*, *144*, 360–383, https://doi.org/https://doi.org/10.1002/qj.3266

Gebrechorkos, S., Pan, M., Beck, H., Sheffield, J. (2022). Performance of state-of-the-art c3s european seasonal climate forecast models for mean and extreme precipitation over africa. *Water Resources Research*, *58*(3), e2021WR031480, https://doi.org/https://doi.org/10.1029/2021WR031480

Giannini, A., Ali, A., Kelley, C., Lamptey, B., Minoungou, B., Ndiaye, O. (2020). Advances in the lead time of sahel rainfall prediction with the north american multimodel ensemble. *Geophysical Research Letters*, *47*(9), e2020GL087341, https://doi.org/https://doi.org/10.1029/2020GL087341

Gibson, P.B., Chapman, W.E., Altinok, A., Delle Monache, L., DeFlorio, M.J., Waliser, D.E. (2021). Training machine learning models on climate model output yields skillful interpretable seasonal precipitation forecasts. *Communications Earth & Environment*, *2*(1), 159, https://doi.org/https://doi.org/10.1038/s43247-021-00225-4

Harmon, G., Jepson, W., Lefore, N. (2023). Farmer-led irrigation development in sub-saharan africa. *Wiley Interdisciplinary Reviews: Water*, *10*(2), e1631, https://doi.org/https://doi.org/10.1002/wat2.1631

Hartmann, H. (2025). Comparison of precipitation rates from global datasets for the five-year period from 2019 to 2023. *Hydrology*, *12*(1), 4, https://doi.org/https://doi.org/10.3390/hydrology12010004

He, S., Li, X., DelSole, T., Ravikumar, P., Banerjee, A. (2020). Sub-seasonal climate forecasting via machine learning: Challenges. *Analysis, and Advances*, ,

He, S., Li, X., DelSole, T., Ravikumar, P., Banerjee, A. (2021). Sub-seasonal climate forecasting via machine learning: Challenges, analysis, and advances. *Proceedings of the aaai conference on artificial intelligence* (Vol. 35, pp. 169–177).

Heilemann, J., Klassert, C., Samaniego, L., Thober, S., Marx, A., Boeing, F., ... Gawel, E. (2024). Projecting impacts of extreme weather events on crop yields using lasso regression. *Weather and Climate Extremes*, *46*, 100738, https://doi.org/https://doi.org/10.1016/j.wace.2024.100738

Hochreiter, S., & Schmidhuber, J. (1997). Long short-term memory. *Neural computation*, *9*(8), 1735–1780, https://doi.org/10.1162/neco.1997.9.8.1735

Hoerl, A.E., & Kennard, R.W. (1970). Ridge regression: Biased estimation for nonorthogonal problems. *Technometrics*, *12*(1), 55–67, https://doi.org/10.1080/00401706.1970.10488634

Hoseini, F., & Notash, A.Y. (2025). Image captioning using bidirectional lstm neural network. *Discover Artificial Intelligence*, *5*(1), 80, https://doi.org/https://doi.org/10.1007/s44163-025-00315-8

Hounnou, F.E., Houessou, A.M., Dedehouanou, H. (2023). Farmers' preference and willingness to pay for weather forecast services in benin (west africa). *Regional*

Environmental Change, *23*(2), 77, https://doi.org/https://doi.org/10.1007/s10113-023-02058-7

Huang, F.L. (2018). Multilevel modeling and ordinary least squares regression: how comparable are they? *The Journal of Experimental Education*, *86*(2), 265–281, https://doi.org/https://doi.org/10.1080/00220973.2016.1277339

Ibebuchi, C.C., & Abu, I.-O. (2023). Rainfall variability patterns in nigeria during the rainy season. *Scientific Reports*, *13*(1), 7888, https://doi.org/https://doi.org/10.1038/s41598-023-34970-7

Ingram, K., Roncoli, M., Kirshen, P. (2002). Opportunities and constraints for farmers of west africa to use seasonal precipitation forecasts with burkina faso as a case study. *Agricultural systems*, *74*(3), 331–349, https://doi.org/https://doi.org/10.1016/S0308-521X(02)00044-6

Izadi, N., Karakani, E.G., Saadatabadi, A.R., Shamsipour, A., Fattahi, E., Habibi, M. (2021). Evaluation of era5 precipitation accuracy based on various time scales over iran during 2000–2018. *Water*, *13*(18), 2538, https://doi.org/https://doi.org/10.3390/w13182538

James, G., Witten, D., Hastie, T., Tibshirani, R. (2013). *An introduction to statistical learning: with applications in r* (Vol. 103). Springer.

Jiang, Y., Zhou, L., Roundy, P.E., Hua, W., Raghavendra, A. (2021). Increasing influence of indian ocean dipole on precipitation over central equatorial africa. *Geophysical Research Letters*, *48*(8), e2020GL092370, https://doi.org/https://doi.org/10.1029/2020GL092370

Jin, W., Luo, Y., Wu, T., Huang, X., Xue, W., Yu, C. (2022). Deep learning for seasonal precipitation prediction over china. *Journal of Meteorological Research*, *36*(2), 271–281, https://doi.org/https://doi.org/10.1007/s13351-022-1174-7

Jingyong, Z., Wenjie, D., Congbin, F., Lingyun, W. (2003). The influence of vegetation cover on summer precipitation in china: A statistical analysis of ndvi and climate data. *Advances in Atmospheric Sciences*, *20*, 1002–1006, https://doi.org/https://doi.org/10.1007/BF02915523

Joshi, S., Gouda, K., Goswami, P. (2020). Seasonal rainfall forecast skill over central himalaya with an atmospheric general circulation model. *Theoretical and Applied Climatology*, *139*, 237–250, https://doi.org/https://doi.org/10.1007/s00704-019-02971-0

Kalnay, E., & Dalcher, A. (1987). Forecasting forecast skill. *Monthly weather review*, *115*(2), 349–356,

Kassem, Y., Gökçekuş, H., Çamur, H., Esenel, E. (2021). Application of artificial neural network, multiple linear regression, and response surface regression models in the estimation of monthly rainfall in northern cyprus. *Desalination and Water Treatment*, *215*, 328–346, https://doi.org/https://doi.org/10.5004/dwt.2021.26525

Kebacho, L.L. (2022a). Interannual variations of the monthly rainfall anomalies over tanzania from march to may and their associated atmospheric circulations anomalies. *Natural Hazards*, *112*(1), 163–186,

Kebacho, L.L. (2022b). The role of tropical cyclones idai and kenneth in modulating rainfall performance of 2019 long rains over east africa. *Pure and Applied Geophysics*, *179*(4), 1387–1401, https://doi.org/https://doi.org/10.1007/s00024-022-02993-2

Kilavi, M., MacLeod, D., Ambani, M., Robbins, J., Dankers, R., Graham, R., ... Todd, M.C. (2018). Extreme rainfall and flooding over central kenya including nairobi city during the long-rains season 2018: causes, predictability, and potential for early warning and actions. *Atmosphere*, *9*(12), 472, https://doi.org/https://doi.org/10.3390/atmos9120472

Kim, G., Ahn, J.-B., Kryjov, V.N., Lee, W.-S., Kim, D.-J., Kumar, A. (2021). Assessment of mme methods for seasonal prediction using wmo lc-lrfmme hindcast dataset. *International Journal of Climatology*, *41*, E2462–E2481, https://doi.org/https://doi.org/10.1002/joc.6858

Kirchner, J.W., & Allen, S.T. (2020). Seasonal partitioning of precipitation between streamflow and evapotranspiration, inferred from end-member splitting analysis. *Hydrology and Earth System Sciences*, *24*(1), 17–39, https://doi.org/https://doi.org/10.5194/hess-24-17-2020

Klemm, T., & McPherson, R.A. (2017). The development of seasonal climate forecasting for agricultural producers. *Agricultural and forest meteorology*, *232*, 384–399, https://doi.org/https://doi.org/10.1016/j.agrformet.2016.09.005

Kumar, V., Kedam, N., Sharma, K.V., Khedher, K.M., Alluqmani, A.E. (2023). A comparison of machine learning models for predicting rainfall in urban metropolitan cities. *Sustainability*, *15*(18), 13724, https://doi.org/https://doi.org/10.3390/su151813724

Li, Y., Wei, K., Chen, K., He, J., Zhao, Y., Yang, G., ... others (2023). Forecasting monthly water deficit based on multi-variable linear regression and random forest models. *Water*, *15*(6), 1075, https://doi.org/https://doi.org/10.3390/w15061075

Lin, X., Fan, J., Hou, Z.J., Wang, J. (2023). Machine learning of key variables impacting extreme precipitation in various regions of the contiguous united states. *Journal of Advances in Modeling Earth Systems*, *15*(3), e2022MS003334, https://doi.org/https://doi.org/10.1029/2022MS003334

Liu, J., Fu, Z., Liu, W. (2023). Impacts of precipitation variations on agricultural water scarcity under historical and future climate change. *Journal of Hydrology*, *617*, 128999, https://doi.org/https://doi.org/10.1016/j.jhydrol.2022.128999

Liu, Z., Wang, Y., Vaidya, S., Ruehle, F., Halverson, J., Soljačić, M., ... Tegmark, M. (2024). Kan: Kolmogorov-arnold networks. *arXiv preprint arXiv:2404.19756*, , https://doi.org/https://doi.org/10.48550/arXiv.2404.19756

Lundberg, S.M., & Lee, S.-I. (2017). A unified approach to interpreting model predictions. *Advances in neural information processing systems*, *30*, , https://doi.org/10.48550/arXiv.1705.07874

MacLeod, D., Graham, R., O'Reilly, C., Otieno, G., Todd, M. (2021). Causal pathways linking different flavours of enso with the greater horn of africa short rains. *Atmospheric Science Letters*, *22*(2), e1015, https://doi.org/https://doi.org/10.1002/asl.1015

Manzanas, R., Gutiérrez, J.M., Bhend, J., Hemri, S., Doblas-Reyes, F.J., Torralba, V., ... Brookshaw, A. (2019). Bias adjustment and ensemble recalibration methods for seasonal forecasting: A comprehensive intercomparison using the c3s dataset.

Climate Dynamics, *53*, 1287–1305, https://doi.org/https://doi.org/10.1007/s00382-019-04640-4

Martin, Z., Son, S.-W., Butler, A., Hendon, H., Kim, H., Sobel, A., ... Zhang, C. (2021). The influence of the quasi-biennial oscillation on the madden–julian oscillation. *Nature Reviews Earth & Environment*, *2*(7), 477–489, https://doi.org/https://doi.org/10.1038/s43017-021-00173-9

Mienye, I.D., & Jere, N. (2024). A survey of decision trees: Concepts, algorithms, and applications. *IEEE access*, *12*, 86716–86727, https://doi.org/https://doi.org/10.1109/ACCESS.2024.3416838

Miftachov, R., & Reiß, M. (2025). Early stopping for regression trees. *arXiv preprint arXiv:2502.04709*, , https://doi.org/https://doi.org/10.48550/arXiv.2502.04709

Misiani, H.O., Endris, H.S., Opijah, F.J., Ouma, J.O., Barasa, B.N., Tye, M.R., MacMartin, D.G. (2025). Simulated response of the climate of eastern africa to stratospheric aerosol intervention. *Frontiers in Climate*, *7*, 1522235, https://doi.org/https://doi.org/10.3389/fclim.2025.1522235

Mohamed, A., Maharana, P., Phartyal, S.S., Dimri, A. (2024). Projected change in precipitation and temperature over undivided sudan and its major cities. *Meteorology and Atmospheric Physics*, *136*(2), 11, https://doi.org/https://doi.org/10.1007/s00703-024-01017-z

Mpelasoka, F., Awange, J.L., Zerihun, A. (2018). Influence of coupled ocean-atmosphere phenomena on the greater horn of africa droughts and their implications. *Science of the Total Environment*, *610*, 691–702, https://doi.org/https://doi.org/10.1016/j.scitotenv.2017.08.109

Mubialiwo, A., Onyutha, C., Abebe, A. (2020). Historical rainfall and evapotranspiration changes over mpologoma catchment in uganda. *Advances in Meteorology*, *2020*(1), 8870935, https://doi.org/https://doi.org/10.1155/2020/8870935

Nhamo, L., Mpandeli, S., Liphadzi, S., Dirwai, T.L., Mugiyo, H., Senzanje, A., ... Mabhaudhi, T. (2024). Why do farmers not irrigate all the areas equipped for irrigation? lessons from southern africa. *Agriculture*, *14*(8), 1218–1218, https://doi.org/https://doi.org/10.3390/agriculture14081218

Nicholson, S.E. (2015). Long-term variability of the east african'short rains' and its links to large-scale factors. *International Journal of Climatology*, *35*(13), , https://doi.org/https://doi.org/10.1002/joc.4259

Noh, S.-H. (2021). Analysis of gradient vanishing of rnns and performance comparison. *Information*, *12*(11), 442, https://doi.org/https://doi.org/10.3390/info12110442

Oettli, P., & Camberlin, P. (2005). Influence of topography on monthly rainfall distribution over east africa. *Climate Research*, *28*(3), 199–212, https://doi.org/https://doi.org/10.3354/cr028199

Pakdaman, M., Babaeian, I., Bouwer, L.M. (2022). Improved monthly and seasonal multi-model ensemble precipitation forecasts in southwest asia using machine learning algorithms. *Water*, *14*(17), 2632, https://doi.org/https://doi.org/10.3390/w14172632

Palmer, P.I., Wainwright, C.M., Dong, B., Maidment, R.I., Wheeler, K.G., Gedney, N., ... others (2023). Drivers and impacts of eastern african rainfall variability. *Nature Reviews Earth & Environment*, *4*(4), 254–270, https://doi.org/https://doi.org/10.1038/s43017-023-00397-x

Paparrizos, S., Attoh, E.M., Sutanto, S.J., Snoeren, N., Ludwig, F. (2023). Local rainfall forecast knowledge across the globe used for agricultural decision-making. *Science of the Total Environment*, *899*, 165539, https://doi.org/https://doi.org/10.1016/j.scitotenv.2023.165539

Pfunzo, R., Bahta, Y.T., Jordaan, H. (2024). Insights into the impact of irrigation agriculture on the economy of the limpopo province, south africa: a social accounting matrix multiplier analysis. *Agriculture*, *14*(7), 1086, https://doi.org/https://doi.org/10.3390/agriculture14071086

Qian, Q., Jia, X., Lin, H., Zhang, R. (2021). Seasonal forecast of nonmonsoonal winter precipitation over the eurasian continent using machine-learning models. *Journal of Climate*, *34*(17), 7113–7129, https://doi.org/https://doi.org/10.1175/JCLI-D-21-0113.1

Reboita, M.S., Mattos, E.V., Capucin, B.C., de Souza, D.O., de Souza Ferreira, G.W. (2024). A multi-scale analysis of the extreme precipitation in southern brazil in april/may 2024. *Atmosphere*, *15*(9), 1123, https://doi.org/10.3390/atmos15091123

Ringler, C., Mekonnen, D.K., Xie, H., Uhunamure, A.M. (2020). Irrigation to transform agriculture and food systems in africa south of the sahara. https://doi.org/https://doi.org/10.2499/9780896293946_06

Sattari, M.T., Feizi, H., Samadianfard, S., Falsafian, K., Salwana, E. (2021). Estimation of monthly and seasonal precipitation: A comparative study using data-driven methods versus hybrid approach. *Measurement*, *173*, 108512, https://doi.org/https://doi.org/10.1016/j.measurement.2020.108512

Schuster, M., & Paliwal, K.K. (1997). Bidirectional recurrent neural networks. *IEEE transactions on Signal Processing*, *45*(11), 2673–2681, https://doi.org/https://doi.org/10.1109/78.650093

Schwarzwald, K., Goddard, L., Seager, R., Ting, M., Marvel, K. (2023). Understanding cmip6 biases in the representation of the greater horn of africa long and short rains. *Climate Dynamics*, *61*(3), 1229–1255, https://doi.org/https://doi.org/10.1007/s00382-022-06622-5

Sheikh, M.R., & Coulibaly, P. (2024). Review of recent developments in hydrologic forecast merging techniques. *Water*, *16*(2), 301, https://doi.org/https://doi.org/10.3390/w16020301

Shetty, S., Umesh, P., Shetty, A. (2022). Dependability of rainfall to topography and micro-climate: an observation using geographically weighted regression. *Theoretical and Applied Climatology*, *147*(1), 217–237, https://doi.org/https://doi.org/10.1007/s00704-021-03811-w

Shu, Z., Zhang, J., Jin, J., Wang, L., Wang, G., Wang, J., ... others (2021). Evaluation and application of quantitative precipitation forecast products for mainland china based on tigge multimodel data. *Journal of Hydrometeorology*, *22*(5), 1199–1219, https://doi.org/https://doi.org/10.1175/JHM-D-20-0004.1

Somvanshi, S., Javed, S.A., Islam, M.M., Pandit, D., Das, S. (2024). A survey on kolmogorov-arnold network. *arXiv preprint arXiv:2411.06078*, , https://doi

.org/https://doi.org/10.48550/arXiv.2411.06078

Song, Y., & Zhang, J. (2024). Enhancing short-term streamflow prediction in the haihe river basin through integrated machine learning with lasso. *Water Science & Technology*, *89*(9), 2367–2383, https://doi.org/https://doi.org/10.2166/wst.2024.142

Taguchi, M. (2018). Seasonal winter forecasts of the northern stratosphere and troposphere: results from jma seasonal hindcast experiments. *Journal of the Atmospheric Sciences*, *75*(3), 827–840, https://doi.org/https://doi.org/10.1175/JAS-D-17-0276.1

Talib, M.N.A., Ahmed, M., Naseer, M.M., Slusarczyk, B., Popp, J. (2021). The long-run impacts of temperature and rainfall on agricultural growth in sub-saharan africa. *Sustainability*, *13*(2), 595, https://doi.org/https://doi.org/10.3390/su13020595

Tibshirani, R. (1996). Regression shrinkage and selection via the lasso. *Journal of the Royal Statistical Society Series B: Statistical Methodology*, *58*(1), 267–288, https://doi.org/10.1111/j.2517-6161.1996.tb02080.x

Van Houdt, G., Mosquera, C., Nápoles, G. (2020). A review on the long short-term memory model. *Artificial Intelligence Review*, *53*(8), 5929–5955, https://doi.org/https://doi.org/10.1007/s10462-020-09838-1

Vapnik, V., Golowich, S., Smola, A. (1996). Support vector method for function approximation, regression estimation and signal processing. *Advances in neural information processing systems*, *9*, , https://doi.org/https://doi.org/10.1007/s10589-017-9975-9

Vellinga, M., & Milton, S.F. (2018). Drivers of interannual variability of the e ast a frican "l ong r ains". *Quarterly Journal of the Royal Meteorological Society*, *144*(712), 861–876, https://doi.org/https://doi.org/10.1002/qj.3263

Vuković Vimić, A., Djurdjević, V., Ranković-Vasić, Z., Nikolić, D., Ćosić, M., Lipovac, A., ... Vujadinović Mandić, M. (2022). Enhancing capacity for short-term climate change adaptations in agriculture in serbia: development of integrated agrometeorological prediction system. *Atmosphere*, *13*(8), 1337, https://doi.org/https://doi.org/10.3390/atmos13081337

Wang, M., Yan, B., Zhang, Y., Zhang, L., Wang, P., Huang, J., ... Wen, Y. (2024). Optimizing precipitation forecasting and agricultural water resource allocation using the gaussian-stacked-lstm model. *Atmosphere*, *15*(11), 1308, https://doi.org/https://doi.org/10.3390/atmos15111308

Wang, Y., Zou, B., Xu, J., Xu, C., Tang, Y.Y. (2025). Alr-ht: A fast and efficient lasso regression without hyperparameter tuning. *Neural Networks*, *181*, 106885, https://doi.org/https://doi.org/10.1016/j.neunet.2024.106885

Ward, N., Walker, D.P., Keane, R.J., Marsham, J.H., Scaife, A.A., Birch, C.E., Maybee, B. (2023). Predictability of the east africa long rains through congo zonal winds. *Atmospheric Science Letters*, *24*(12), e1185, https://doi.org/https://doi.org/10.1002/asl.1185

Watson, G.S. (1964). Smooth regression analysis. *Sankhyā: The Indian Journal of Statistics, Series A*, 359–372,

Xhabafti, M., Vika, B., Sinaj, V. (2024). A comparative study of statistical and deep learning model-base weather prediction in albania. *WSEAS Transactions on Computer Research*, *12*, 151–160, https://doi.org/10.37394/232018.2024.12.15

Zhang, Q., Sun, P., Singh, V.P., Chen, X. (2012). Spatial-temporal precipitation changes (1956–2000) and their implications for agriculture in china. *Global and Planetary Change*, *82*, 86–95, https://doi.org/https://doi.org/10.1016/j.gloplacha.2011.12.001